PASSIVE EARTH PRESSURES WITH VARIOUS WALL MOVEMENTS

By Yung-Show Fang,[1] Associate Member, ASCE, Tsang-Jiang Chen,[2] and Bin-Ferng Wu[3]

ABSTRACT: This paper presents experimental data of earth pressure acting against a vertical rigid wall, which moved into a mass of dry sand with a stress-free horizontal surface under various wall-movement modes. To investigate the variation of earth pressure induced by the rotation about a point above the top (RTT) and rotation about a point below the wall base (RBT) types of wall movement, the instrumented retaining-wall facility was developed at National Chiao Tung University. Based on experimental data it is found that, for a wall under translational movement, the passive pressure distribution is linear and in good agreement with Terzaghi's prediction based on the general wedge theory. For a wall under either RTT or RBT mode, the magnitude of passive thrust and its point of application are significantly affected by the mode of wall displacement. However, if the parameter n indicating location of the center of rotation is greater than 2.0, the influence of movement mode on passive earth pressure becomes less important.

INTRODUCTION

The calculation of the forces exerted by soils against structures was one of the earliest problems in soil mechanics. The most widely accepted theories to estimate earth pressure are those of Coulomb and Rankine. However, the earth pressures obtained from these theories do not distinguish between modes of wall movement, and the theories provide no prefailure information.

Important and valuable experimental work associated with earth pressure has been conducted by Terzaghi (1932), Schofield (1961), Matteotti (1970), Bros (1972), Sherif and Mackey (1977), Sherif et al. (1984), Duncan and Seed (1986), Fang and Ishibashi (1986), and Ducan et al. (1991). Unfortunately, most of the work was concerned with at-rest and active pressures. Only the work by Rowe and Peaker (1965), Mackey and Kirk (1967), Narain et al. (1969), and James and Bransby (1970) was associated with passive pressure. Their findings indicate that the passive pressure generated is highly dependent on the assumed mode of wall movement. Note that all of the investigations aforementioned were limited to a few particular modes of wall deformation, namely, horizontal translation (T mode), rotation about the wall top (RT mode), and rotation about the base (RB mode). From a practical point of view, these modes cannot represent the range of movements of retaining walls in the field.

As indicated in Fig. 1, if a straight line is extended along the surface of the wall at a passive state, the extension will intersect the vertical line at

[1]Assoc. Prof., Dept. of Civ. Engrg., Nat. Chiao Tung Univ., Hsinchu, Taiwan, 30050, Republic of China.

[2]Grad. Student, Dept. of Civ. Engrg., Nat. Chiao Tung Univ., Hsinchu, Taiwan, 30050, Republic of China.

[3]Grad. Student, Dept. of Civ. Engrg., Nat. Chiao Tung Univ., Hsinchu, Taiwan, 30050, Republic of China.

Note. Discussion open until January 1, 1995. To extend the closing date one month, a written request must be filed with the ASCE Manager of Journals. The manuscript for this paper was submitted for review and possible publication on July 26, 1993. This paper is part of the ***Journal of Geotechnical Engineering***, Vol. 120, No. 8, August, 1994. ©ASCE, ISSN 0733-9410/94/0008-1307/$2.00 + $.25 per page. Paper No. 6648.

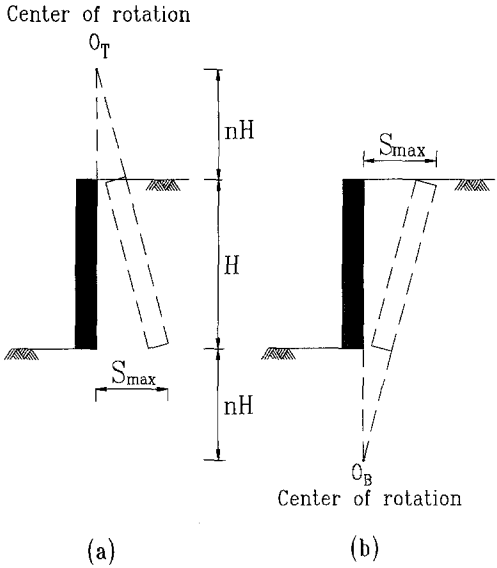

FIG. 1. Two Types of Passive Wall Movements: (*a*) RTT Mode; (*b*) RBT Mode

point O_T or O_B. In this respect, the wall movement could be considered as a rotation about the center, O_T or O_B. Note in Fig. 1 that n is the parameter indicating location of the center of rotation, and the general movements of a rigid wall moving toward the backfill could be included into the following two categories:

1. Rotation about a point above the top (RTT)—It is clear from Fig. 1(*a*) that when n equals zero, this becomes the RT mode. On the other hand, as n approaches infinity, this becomes the translational wall movement. Therefore, this category of movement is abbreviated as the RTT mode.
2. Rotation about a point below the wall base (RBT)—In this mode, the soil behavior in front of the toe of an overturning or sliding retaining wall is simulated. It may be seen from Fig. 1(*b*) that when n equals zero this is the RB mode. This category of movement is termed the RBT mode. Nevertheless, the movement of a real retaining wall is complicated and depends mainly on the wall rigidity, construction method, and support conditions provided.

To investigate the variation of earth pressure induced by various wall movements, the instrumented retaining-wall facility was developed at National Chiao Tung University (NCTU). All of the earth-pressure experiments described in this article were conducted in the NCTU retaining-wall facility, which is introduced in the following section. This paper presents experimental data of earth pressure acting against an initially vertical wall, which moves into a mass of dry sand with a stress-free horizontal surface under RTT and RBT movement modes. With the soil-pressure transducers (SPT) mounted on the model wall, measurements were made for the normal stresses against the wall. Due to the scale effect, it may not be appropriate

to predict the behavior of large walls from the results obtained from small-scale models. However, the test findings should result in a better understanding regarding the effect of wall movement on the development of earth pressure. It is also hoped that the experimental data will provide a comprehensive and reliable basis for evaluating the validity of miscellaneous theories and analytical procedures that have been developed to calculate the earth pressure.

NCTU RETAINING-WALL FACILITY

The entire facility consists of four components, namely, model retaining wall, soil bin, driving system, and data acquisition system.

Model Retaining Wall

The movable model retaining wall and its driving system are illustrated in Fig. 2. The model wall is a 1,000-mm-wide, 550-mm-high, and 120-mm-thick solid plate, and is made of steel. Note (Fig. 2) that the effective wall height H (or height of backfill above wall base) is only 500 mm. The retaining wall is vertically supported by two unidirectional rollers, and is laterally supported by four driving rods. Two sets of wall-driving mechanisms, one for the upper rods and the other for the lower rods, provide various kinds of movements for the wall. The 1,000-mm-wide, 337-mm-high, and 120-mm-thick steel plate on top of the movable wall is designed to resist the uplift component of passive earth pressure. Two 45° notches have been grooved at the bottom of the model wall, and another two notches have been cut on top of the fixed bed below the wall. The two 30-mm-diameter

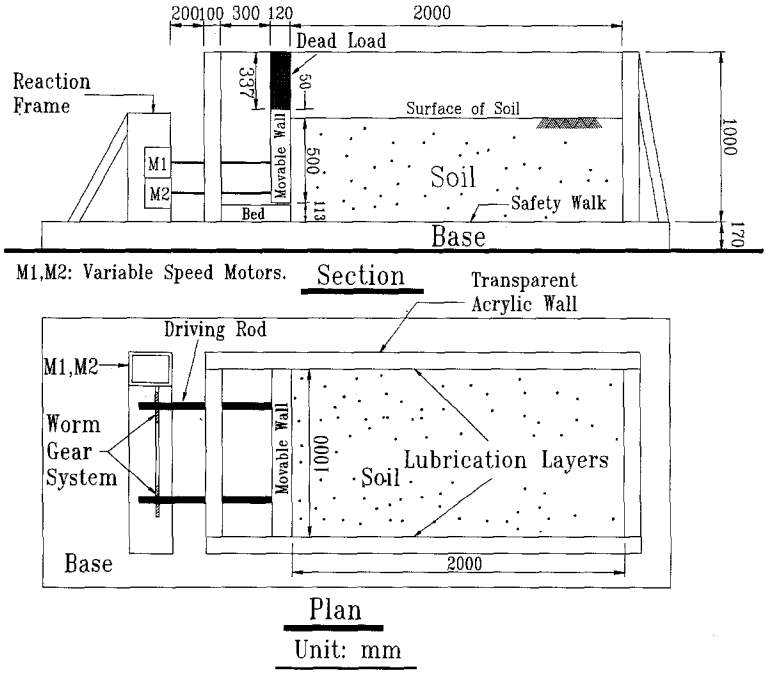

FIG. 2. NCTU Retaining-Wall Facility

steel balls act like unidirectional rollers, which permit wall motion only in the direction perpendicular to the wall surface.

To investigate the distribution of earth pressure, soil-pressure transducers are attached to the model retaining wall as shown in Fig. 3. Ten strain-gage-type transducers (Kyowa BE-2KRS17 and BE-5KRS17) have been arranged within the central zone of the wall. Another three transducers (SPT10, 11, and 12) have been mounted between the central zone and sidewall to investigate the variation of the sidewall effect. To eliminate the soil-arching effect, all earth-pressure transducers are quite stiff, and are installed flush with the face of the wall. Calculation based on Coulomb's passive earth-pressure theory indicates that the maximum deflection for the 120-mm-thick steel wall is only 0.00044 mm.

Soil Bin

The soil bin is fabricated of steel members with inside dimensions of 2,000 mm × 1,000 mm × 1,000 mm (see Fig. 2). Both sidewalls of the soil bin are made of 30-mm-thick transparent acrylic plates through which the behavior of backfill can be observed. Outside the acrylic plates, steel stiffeners are used to confine the sidewalls to ensure a plane strain condition. The bottom of the soil bin is covered with a layer of SAFETY WALK to provide adequate friction between the soil and the base of the bin. According to the general wedge theory (Terzaghi 1941), the passive failure surface developed in the backfill would extend below the base of the wall. As shown in Fig. 2, the fixed bed located below the wall serves to hold the bottom 113 mm of soil to accommodate the entire log-spiral failure surface.

The selection of the width of the soil bin is governed by the friction effect along the sidewalls. Terzaghi (1932) found, by means of experiments on several model retaining walls of equal height and different lengths, that the intensity of the earth pressure is practically independent of the length of the wall (inside width of soil bin), provided that the length of the wall exceeds twice the wall height. For this reason, it has been decided to set the width W of the soil bin equal to twice the height of the wall (W = 1.0 m).

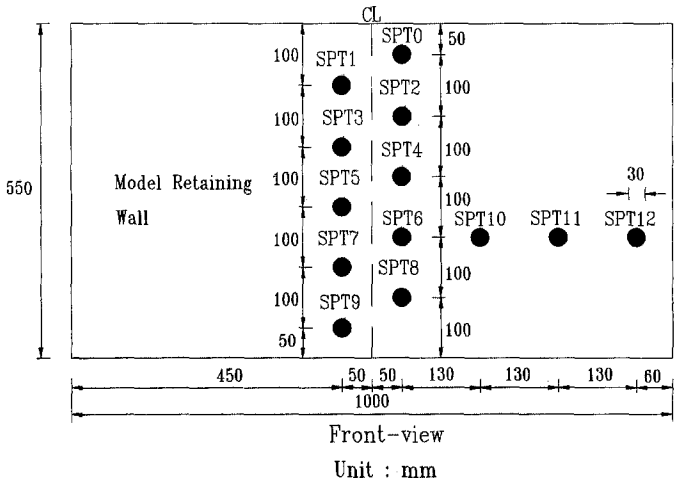

FIG. 3. Locations for Soil-Pressure Transducers

Driving System

As illustrated in Fig. 2, the variable speed motors M1 and M2 (Electro, M4621AB) are employed to compel the upper and lower driving rods, respectively. The shaft rotation compels the worm gear linear actuators, while the actuator would push or pull the driving rods. The motor speeds for M1 and M2 are controlled by two independent sets of automatic-speed-control systems (DIGILOK, DLC-300). The maximum strokes for the driving rods are ± 110 mm.

Data-Acquisition System

Due to the considerable amount of data collected by the soil-pressure transducers, a data-acquisition system is used. The analog signals from the sensors are digitized by an analog-to-digital converter. The digital data are then stored and processed by a microcomputer. For more details regarding the development of NCTU retaining-wall facility, the reader is referred to Wu (1992).

BACKFILL AND INTERFACE CHARACTERISTICS

Air-dry Ottawa sand (ASTM C-109) was used throughout this investigation. Physical properties of the soil include $G_s = 2.65$; $e_{max} = 0.76$; $e_{min} = 0.50$; $D_{60} = 0.36$ mm; and $D_{10} = 0.23$ mm. For this study, the backfill was deposited by air pluviation from the slit of a hopper into the soil bin. The drop distance was kept to be approximately 600 mm to the soil surface through the placement process. Since the pluviation work was conducted manually, a certain degree of heterogeneity in the backfill was inevitable. To investigate the possible scattering of density in the pluviated soil mass, several density-control boxes with inside dimensions of 150 mm $\times$ 150 mm $\times$ 150 mm were used to measure the local densities at different locations and depths. Experimental results indicate that about $\pm 0.5\%$ of scattering in soil density was possible. The soil unit weight achieved with the pluviation method was 15.5 kN/m^3. The corresponding internal friction angle ϕ determined from direct shear tests with normal stresses less than 40 kPa was found to be 30.9°. To limit the scope of this study, only one density was used throughout all experiments.

To reduce the friction between sidewall and backfill, a lubrication layer was furnished for the earth-pressure experiments. The layer consists of a 0.2-mm-thick latex rubber membrane and a thin layer of silicone grease (Shin-etsu KS-63G). The frictional resistance developed between the sidewall and Ottawa sand was evaluated by a special direct shear test. In the test, an acrylic plate (same material as the sidewall) was placed under the upper shear box. Following the testing method suggested by Tatsuoka and Haibara (1985), the friction angles at the interface under different normal stresses are plotted in Fig. 4. It is clear from these data that the friction angle decreases with increasing normal stress. If the normal stress is greater than 40 kN/m^2, the friction angle could be successfully reduced to less than 1°. However, if the normal stress at the interface is less than 10 kN/m^2, the friction angle becomes significantly higher. By replacing the acrylic plate with a steel plate (same material as the model wall) and removing the lubrication layer, the friction angle δ between Ottawa sand ($\gamma = 15.5$ kN/m^3) and steel is found to be 19.2°. The ϕ and δ angles determined from the tests are assumed for the calculation of earth pressure for the Coulomb, Rankine, and Terzaghi theories in the following sections.

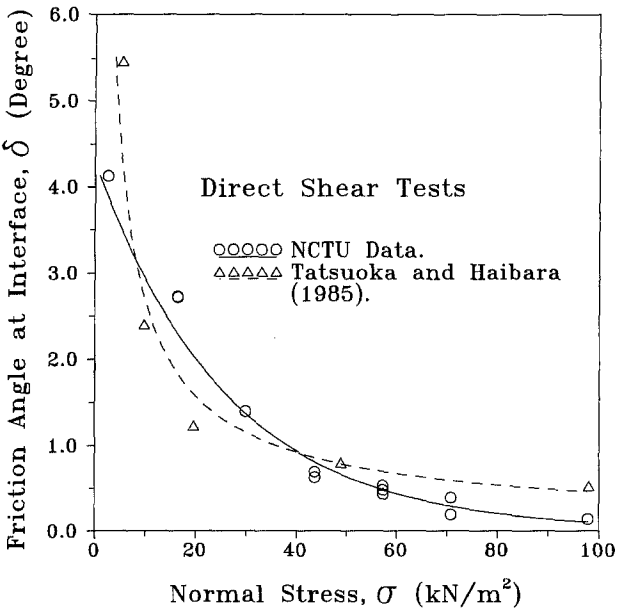

FIG. 4. Measured Friction Angle δ with Different Normal Stresses for Acrylic Plate Lubricated with Silicone Grease

TEST RESULTS

Translational Wall Movement

After the backfill had been placed into the soil bin, the model wall slowly moved toward the soil mass at a constant speed of 0.27 mm/s. The distributions of earth pressure at different stages of wall movement (S_{max}/H) are shown in Fig. 5. As the wall started to move into soil mass, the earth pressure increased and eventually a limiting passive pressure was reached. A passive state was reached at different depths nearly simultaneously, and the pressure distributions are essentially linear at each stage of deformation up to failure. This finding is in good agreement with the test data reported by Rowe and Peaker (1965).

As illustrated in Fig. 6, the horizontal earth-pressure coefficient (K_h) increases with increasing wall movement and finally a constant total thrust is reached. The coefficient K_h is defined as the ratio of the horizontal component of total thrust to $\gamma H^2/2$. The ultimate value of K_h is defined as the passive earth-pressure coefficient $K_{p,h}$. For the four sets of data shown in Fig. 6, the passive condition occurred at the wall movement of approximately $S_{max}/H = 0.18$. The passive thrust P_h is calculated by summing the earth pressure acting on the wall. For comparison purposes, the passive earth-pressure coefficients determined from Coulomb, Rankine, and Terzaghi theories are also demonstrated in Fig. 6. It is clear that Rankine's theory (assuming $\delta = 0$) underestimates the passive thrust, while Coulomb's theory overestimates the passive pressure. It is found that the experimental $K_{p,h}$ values are in good agreement with Terzaghi's prediction based on the general wedge theory. Experimental data shown in Fig. 7 indicate that resultant forces are located at about $0.36H$ above the wall base. It should

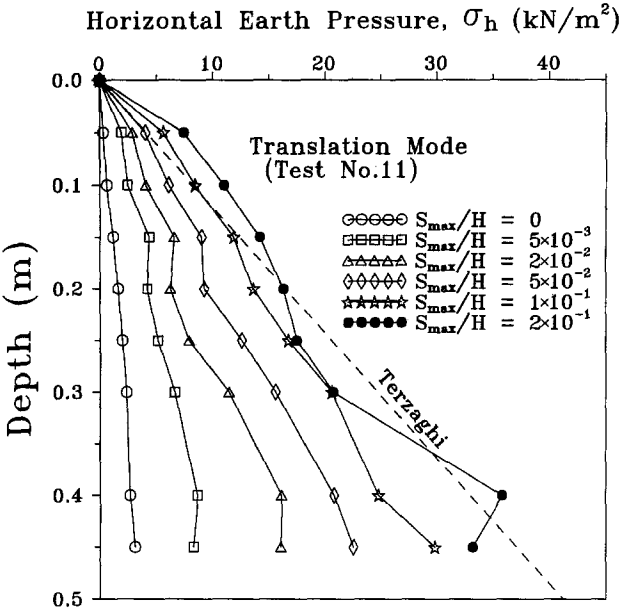

FIG. 5. Distribution of Horizontal Earth Pressure for Translation Mode

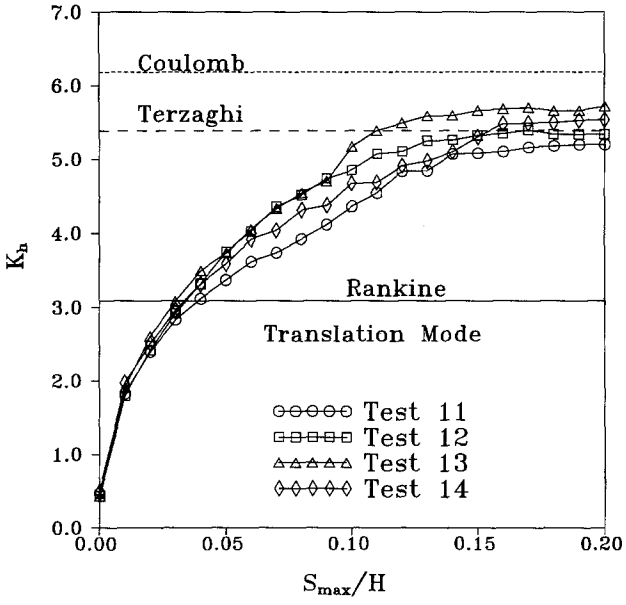

FIG. 6. Variation of K_h with Wall Movement for Translation Mode

be mentioned that, due to the large inherent variability in earth pressures, erroneous evaluations could be possible if too few measurements are made.

Test results obtained under translational wall movement have also been used to evaluate the effect of sidewall friction. Four soil-pressure transducers

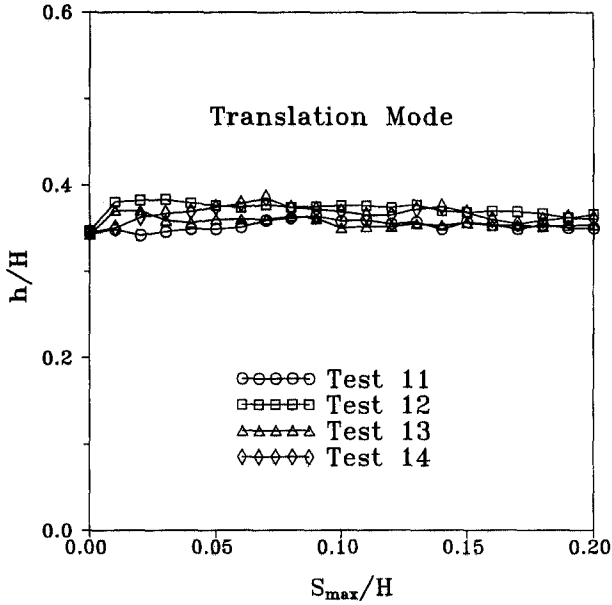

FIG. 7. Variation of Point of Application of Total Thrust with Wall Movement

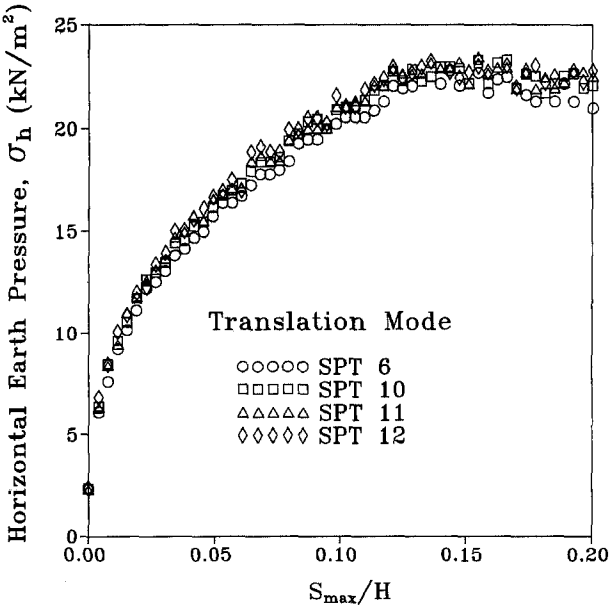

FIG. 8. Comparison of Earth Pressures Measured at Different Distances from Sidewall

(SPT6, SPT10, SPT11, and SPT12) are installed on the model wall at the same elevation across the wall face. Experimental data plotted in Fig. 8 shows that, with the lubrication layers, earth pressures measured at different distances from the sidewall are in fairly good agreement. However, due to the slight friction near the sidewall, the passive resistance measured at SPT12 is slightly greater than those measured at other cells.

RTT Wall Movement

The variations of horizontal earth pressure (σ_h) measured at different depths as a function of wall movement ($n = 0.00$) are shown in Fig. 9. It may be observed from these data that the pressure measured near the lower edge of the wall (SPT9) increased rapidly with increasing wall rotation before reaching an ultimate value. However, the pressure measured near the top (SPT1) did not change so significantly. Fig. 10(*a*) shows the pressure distributions at various movement stages. For this case, maximum lateral displacement occurred at the wall base, while no lateral movement was allowed at the top. As a result, the earth pressure measured near the wall base increased rapidly with the passive wall movement while pressure near the top remained nearly unchanged. At the wall movement of $S_{max}/H = 0.20$, the pressure distribution obtained is far from linear.

The variation of the earth pressure coefficient with wall motion for $n = 0.00$ is indicated in Fig. 11. In the figure, K_h increases with increasing wall movement then gradually the tendency to increase slows down as S_{max}/H approaches 0.20. In comparison with the $K_{p,h}$ coefficients determined from Coulomb, Rankine, and Terzaghi theories, the measured data are lower. This occurs because the backfill near the upper portion of the wall did not yield sufficiently to cause a passive state. It should be mentioned that the passive earth pressure is commonly employed to resist the motion of a

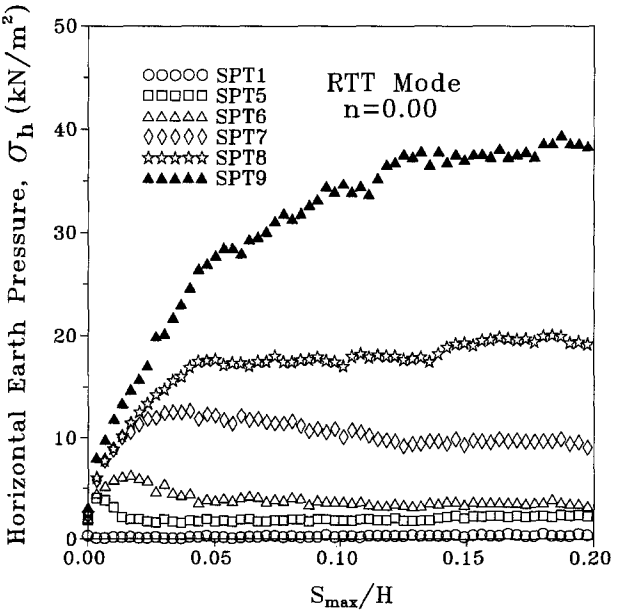

FIG. 9. Variation of Horizontal Earth Pressure with RTT Wall Movement

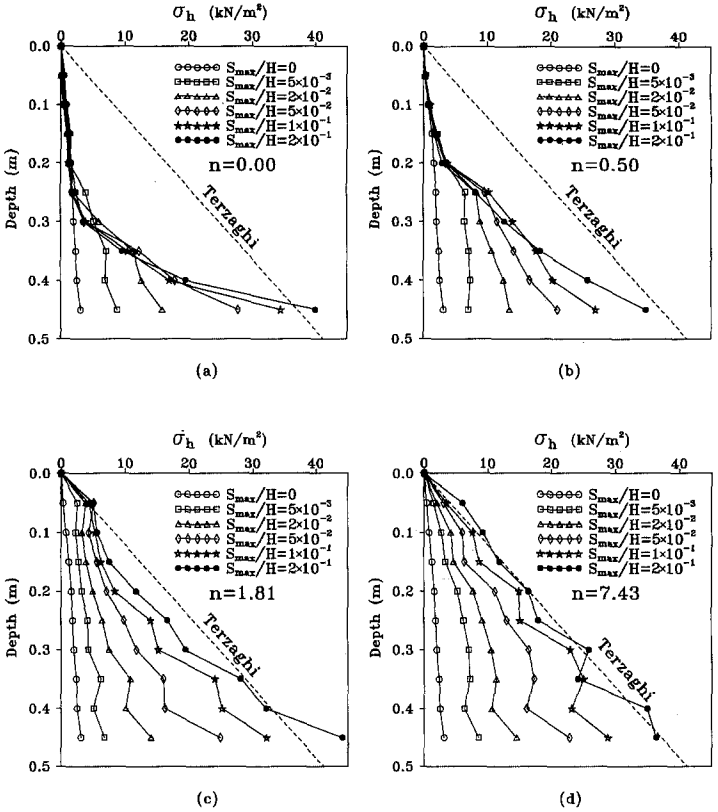

FIG. 10. Distribution of Horizontal Earth Pressure for RTT Mode

structure, such as an anchor plate or retaining wall. The overestimation of passive thrust would result in a reduction of the safety factor for the structure. Fig. 12 shows, with the wall movement, the point of application of total thrust gradually moved down to about $0.18H$ above the wall base and then remained almost unchanged.

Figs. 10(b–d) show the earth-pressure distribution for $n = 0.50$, 1.81, and 7.43, respectively. As the parameter n increases, more lateral compression is allowed in soil mass near the upper portion of the wall, therefore more significant pressure variation was measured. Consequently, the earth pressure induced is closer to that induced by a translational wall movement. The variations of K_h with wall motion for various n values are summarized in Fig. 11. It is clear from the figure that K_h increases with increasing wall movement before reaching a stable value. For the group of relationships shown, test data for $n = 0.00$ become the lower bound, while those for the T mode become the upper bound. The variations of point of application of resultant force as a function of wall movement for various n values are summarized in Fig. 12. It may be seen from these data that, with an increasing n value, the curve gradually converges to that for the T mode.

Assuming the effect of the S_{max}/H parameter is similar for other wall heights, for a 5.0-m-high retaining wall, the wall movement of $S_{max}/H = 0.20$ corresponds to 1.0 m of lateral wall displacement. It appears that further

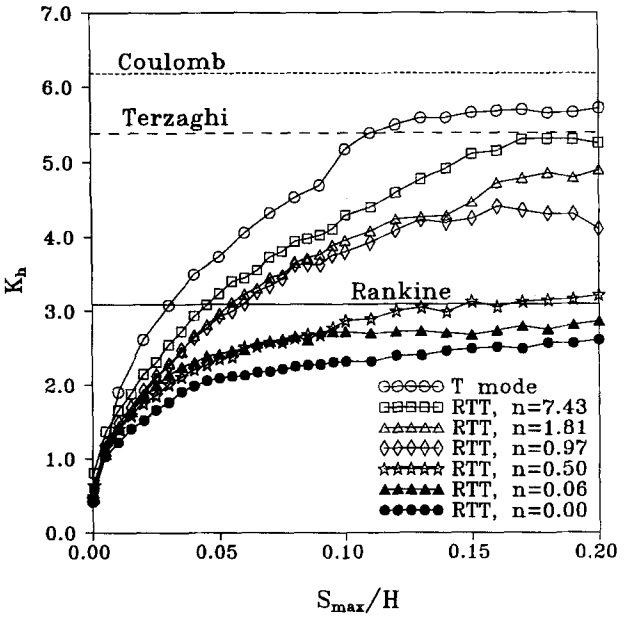

FIG. 11. Variation of K_h with Wall Movement for RTT Mode

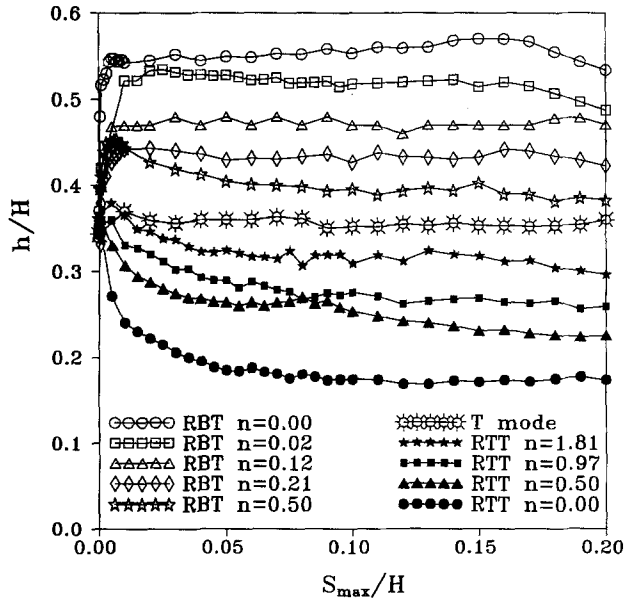

FIG. 12. Relationship between h/H and n

wall movement would probably be impractical. On the other hand, the magnitude of total thrust and its point of application have achieved relative stable values at $S_{max}/H = 0.20$. Therefore, for this study, it is defined that a passive state has been reached at the wall movement of $S_{max}/H = 0.20$.

RBT Wall Movement

The earth pressure distributions corresponding to different stages of wall displacements for $n = 0.00$ are shown in Fig. 13(a). It is clear from the test data that the soil pressure measured near the top (SPT1 and SPT2) increased with increasing wall movement, while the change of stress detected near the wall base (SPT9) was quite small. Note that the stresses monitored near midheight of the wall (SPT4 and SPT5) rose continually with increasing wall movement. Test data revealed that, up to $S_{max}/H = 0.20$, the tendency to rise did not stop. The passive pressure distribution shown is clearly nonlinear.

The variation of total thrust as a function of wall movement for $n = 0.00$ is indicated in Fig. 14. The K_h value continually increased with wall rotation. Within the testing range, there does not exist an ultimate value for K_h. Since high stresses were measured near the midheight of the wall, the point of application of passive thrust (P_p) was found to act at about $0.55H$ above the wall base, as shown in Fig. 12.

Figs. 13(b–d) show the earth-pressure distribution for $n = 0.21$, 0.50, and 13.78, respectively. As the n value increases, more lateral displacement is allowed near the wall base, therefore higher stresses are measured there. The variations of resultant force as a function of wall motion for different n values are summarized in Fig. 14. It can be seen from the figure that, as

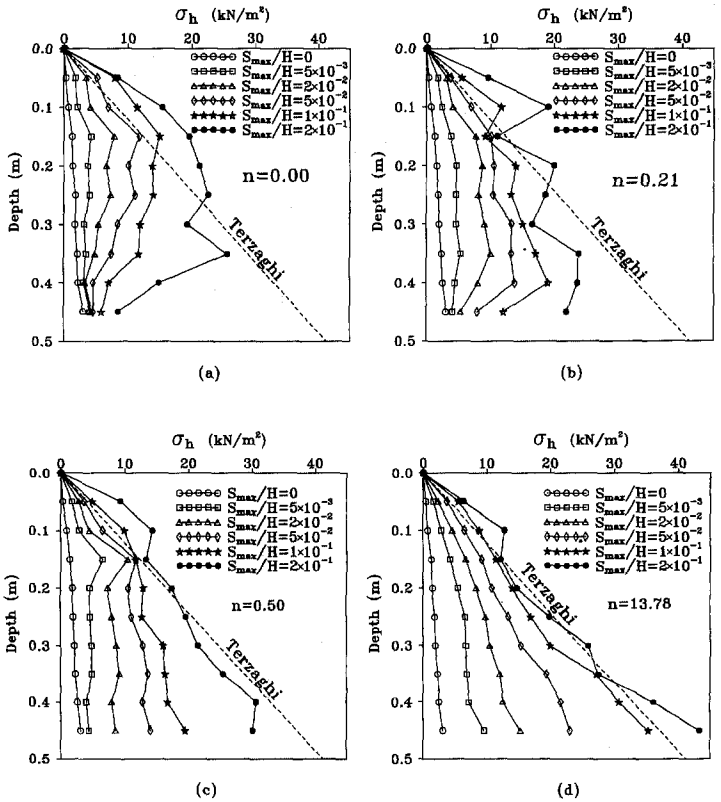

FIG. 13. Distribution of Horizontal Earth Pressure for RBT Mode

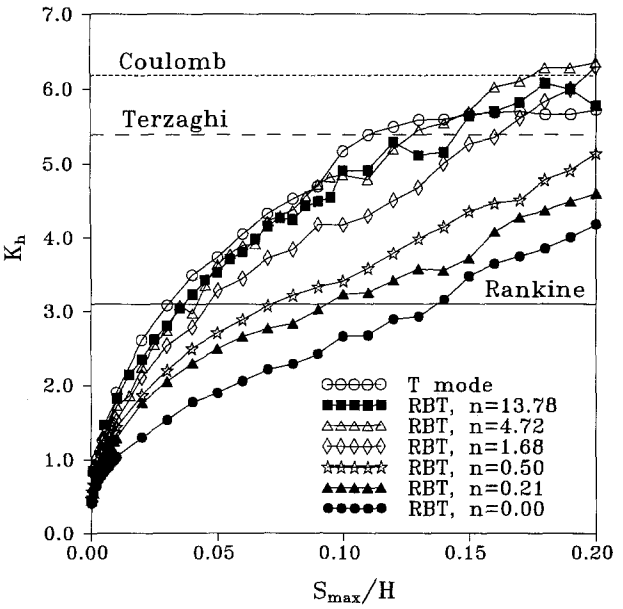

FIG. 14. Variation of K_h with Wall Movement for RBT Mode

n increases, the K_h versus S_{max} curve moves upward. For $n = 1.68$, the ultimate K_h value even exceeded the coefficient $K_{p,h}$ induced by the T mode. However, as n increased further ($n = 4.72$ and $n = 13.78$), the test curve gradually converged to that for the T mode. Fig. 12 summarizes the family of relationships between h/H and S_{max}/H. For the RBT group of curves it may be seen that the relationship for $n = 0.00$ forms the upper bound, while that for the T mode becomes the lower bound.

Comparison Among Different Modes

From an engineering point of view, it is important to determine both the magnitude and the point of application of the total passive thrust. The passive earth-pressure coefficient $K_{p,h}$ as a function of n for both the RTT and RBT modes is presented in Fig. 15. It may be observed from these data that, if the n value is small, the magnitude of P_p is quite sensitive to the change of parameter n. However, if n is greater than about 2.0, the influence of n upon total thrust becomes less significant. Eventually, as n approaches a large number, the $K_{p,h}$ induced by both categories of wall motion would converge to Terzaghi's solution. The point of application of passive thrust for different n values are indicated in Fig. 16. It may be seen from these data that, as parameter n increases, the passive thrust gradually moves to about $H/3$ above the wall base. It may be concluded that, for n values less than about 2.0, the mode of wall movement has an evident influence on the point of application of the passive thrust. However, for n values greater than 2.0, the mode has a limited effect on the point of application of P_p.

To investigate the displacement field in the backfill, a group of 50-mm-spaced grids were plotted on the transparent sidewall, and another group of 50-mm-spaced grids were plotted on the rubber membrane at corresponding positions. Since the sidewall effect has been effectively minimized,

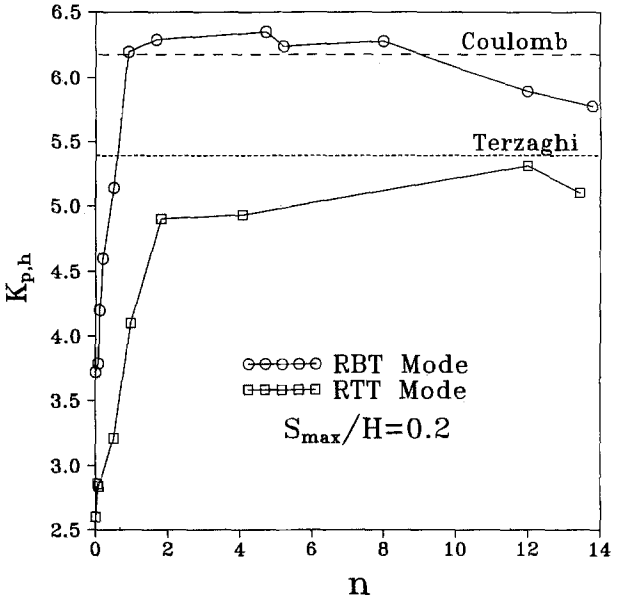

FIG. 15. Relationship between $K_{p,h}$ and n

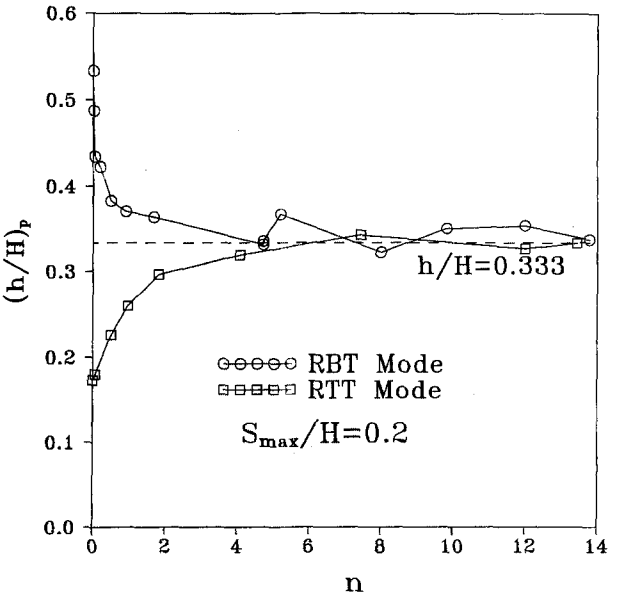

FIG. 16. Relationship between $(h/H)_p$ and n

the membrane should be able to move quite freely with the backfill. Before testing, the grids on the membrane were aligned with those on the sidewall. After the experiment was completed, a wall movement of $S_{max}/H = 0.20$ was achieved, then the movement between the grid point on the membrane

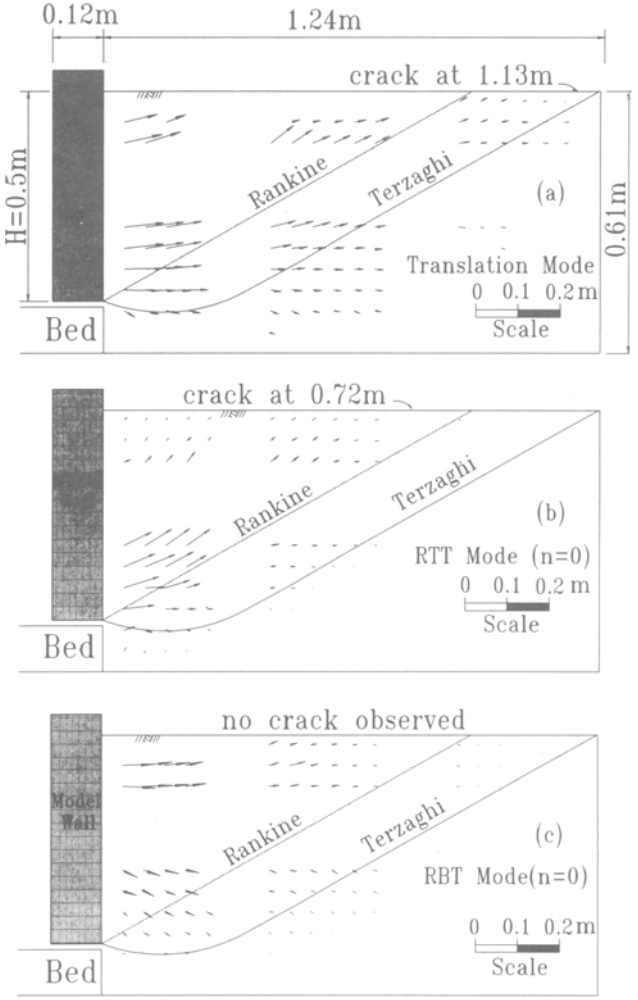

FIG. 17. Accumulated Displacement Vectors for $S_{max}/H = 0.2$

and the point on the sidewall was recorded.

Fig. 17(*a*) shows the displacement vectors of backfill induced by the *T* mode. It is clear that the largest displacements occurred in front of the wall. The soils above the wall base tend to move downward and soils below the wall base tend to move downward. Unfortunately, rupture surfaces determined based on Rankine and Terzaghi theories are not able to define the backfill movements properly. A surface crack was observed at 1.13 m from the wall, which is quite close to Terzaghi's prediction. Displacement vectors observed for the RTT and RBT modes ($n = 0.00$) are shown in Figs. 17(*b*) and (*c*), respectively. From these observations, it may be concluded that backfill displacement is strongly influenced by the movement mode of the wall.

CONCLUSIONS

Based on the experimental data obtained during this investigation, the following conclusions can be drawn about earth pressure acting on a rigid wall that moves toward a backfill of dry sand.

For a wall under translational movement, the pressure distribution is essentially hydrostatic at each stage of wall motion. The passive state is reached at different depths of soil mass nearly simultaneously. The passive earth-pressure coefficient $K_{p,h}$ is found to be in good agreement with Terzaghi's prediction based on general wedge theory.

For a wall under RTT movement modes ($n = 0.00$), the passive pressure distribution obtained is far from linear. The measured passive thrust P_p is apparently lower than those calculated with Coulomb, Rankine, and Terzaghi theories, and its point of application was found at about $0.18H$ above the wall base. As parameter n increases, the earth pressure induced was closer to that induced by the T mode.

For a wall under RBT mode ($n = 0.00$), high stresses were measured near the midheight of the wall, and the passive pressure distribution is nonlinear. The total force increases with increasing wall movement continually, and no ultimate soil thrust was observed up to $S_{max}/H = 0.20$. Due to the stress concentration near the midheight of wall, the point of application of P_p was found to act at about $0.55H$ above the wall base. As n value increases, the earth pressure measured converged to that induced by T mode.

In the n value is small, the magnitude of the passive thrust and its point of application are significantly affected by the wall-movement mode, and are quite sensitive to the change of parameter n. However, if n is greater than about 2.0, the influence of the wall-movement mode upon passive thrust becomes less important.

ACKNOWLEDGMENT

The writers wish to acknowledge the National Science Council of the Republic of China government (NSC 82-0115-E-009-383) for the financial assistance that made this investigation possible.

APPENDIX I. REFERENCES

Bros, B. (1972). "The influence of model retaining wall displacements on active and passive earth pressure in sand." *Proc., 5th Eur. Conf. on Soil Mech.*, Vol. 1, Madrid, 241–249.

Duncan, J. M., and Seed, R. B. (1986). "Compaction-induced earth pressures under K_o condition." *J. Geotech. Engrg.*, ASCE, 112(1), 1–22.

Duncan, J. M., Williams, G. W., Sehn, A. L., and Seed, R. B. (1991). "Estimation earth pressures due to compaction." *J. Geotech. Engrg.*, ASCE, 117(12), 1833–1847.

Fang, Y. S., and Ishibashi, I. (1986). "Static earth pressures with various wall movements." *J. Geotech. Engrg.*, ASCE, 112(3), 317–333.

James, R. G., and Bransby, P. L. (1970). "Experimental and theoretical investigations of a passive pressure problem." *Geotechnique*, 20(1), 17–37.

Mackey, R. D., and Kirk, D. P. (1967). "At rest, active and passive earth pressures." *Proc., South East Asian Conf. on Soil Mech. and Found. Engrg.*, Bangkok, 187–199.

Matteotti, G. (1970). "Some results of quay-wall model tests on earth pressure." *Proc.*, Institution of Civil Engineers, London, England, 47, 185–204.

Narain, J., Saran, S., and Nandakumaran, P. (1969). "Model study of passive pressure in sand." *J. Soil Mech. and Found. Engrg. Div.*, ASCE, 95(4), 969–983.
Rowe, P. W., and Peaker, K. (1965). "Passive earth pressure measurements." *Geotechnique*, 15(1), 57–78.
Schofield, A. N. (1961). "The development of lateral force of sand against the vertical face of a rotating model foundation." *Proc., 5th Int. Conf. Soil Mech. and Found. Engrg.*, Paris, Vol. 2, 479–484.
Sherif, M. A., Fang, Y. S., and Sherif, R. I. (1984). "K_a and K_o behind rotating and nonyielding walls." *J. Geotech. Engrg.*, ASCE, 110(1), 41–56.
Sherif, M. M., and Mackey, R. D. (1977). "Pressures on retaining wall with repeated loading." *J. Geotech. Engrg. Div.*, ASCE, 103(11), 1341–1345.
Tatsuoka, F., and Haibara, O. (1985). "Shear resistance between sand and smooth or lubricated surface." *Soils and Found.*, 25(1), 89–98.
Terzaghi, K. (1932). "Record earth pressure testing machine." *Engrg. News Record*, 109(Sept. 29), 365–369.
Terzaghi, K. (1941). "General wedge theory of earth pressure." *ASCE Trans.*, 68–80.
Wu, B. F. (1992). "Design and construction of National Chiao Tung University model retaining wall." Masters in Engineering thesis, National Chiao Tung University, Hsinchu, Taiwan.

APPENDIX II. NOTATION

The following symbols are used in this paper:

D_{10}, D_{60} = soil diameters of which 10% and 60% of soil by weight is finer;
e_{max}, e_{min} = maximum and minimum void ratio of soil;
G_s = specific gravity of soil;
h = distance between point of application of total resultant force and wall base;
H = height of backfill from wall base;
K_h = coefficient of horizontal soil thrust;
$K_{p,h}$ = coefficient of passive horizontal soil thrust;
n = parameter indicating location of center of rotation;
P_p = resultant of passive earth pressure;
S_{max} = maximum lateral wall displacement;
W = width of soil bin;
γ = unit weight of soil;
δ = friction angle at soil-wall interface;
σ_h = horizontal earth pressure; and
ϕ = internal friction angle of soil.